

# A physiology–based parametric imaging method for FDG–PET data.

Mara Scussolini<sup>1</sup>, Sara Garbarino<sup>2</sup>, Gianmario Sambuceti<sup>3</sup>,  
Giacomo Caviglia<sup>1</sup> and Michele Piana<sup>4</sup>

<sup>1</sup> Dipartimento di Matematica, Università di Genova, Genova, Italy

<sup>2</sup> Centre for Medical Image Computing, Department of Computer Science, University College London, UK

<sup>3</sup> Dipartimento di Medicina Nucleare, IRCCS-IST San Martino, and Dipartimento di Scienze della Salute, Università di Genova, Genova, Italy.

<sup>4</sup> Dipartimento di Matematica, Università di Genova, and CNR-SPIN, Genova, Italy.

E-mail: scussolini@dima.unige.it

*Keywords:* numerical inverse problems, parametric imaging, compartmental analysis, nuclear medicine data

**Abstract.** Parametric imaging is a compartmental approach that processes nuclear imaging data to estimate the spatial distribution of the kinetic parameters governing tracer flow. The present paper proposes a novel and efficient computational method for parametric imaging which is potentially applicable to several compartmental models of diverse complexity and which is effective in the determination of the parametric maps of all kinetic coefficients. We consider applications to  $^{18}\text{F}$ -fluorodeoxyglucose Positron Emission Tomography (FDG–PET) data and analyze the two–compartment catenary model describing the standard FDG metabolism by an homogeneous tissue and the three–compartment non–catenary model representing the renal physiology. We show uniqueness theorems for both models. The proposed imaging method starts from the reconstructed FDG–PET images of tracer concentration and preliminarily applies image processing algorithms for noise reduction and image segmentation. The optimization procedure solves pixelwise the non–linear inverse problem of determining the kinetic parameters from dynamic concentration data through a regularized Gauss–Newton iterative algorithm. The reliability of the method is validated against synthetic data, for the two–compartment system, and experimental real data of murine models, for the renal three–compartment system.

## 1. Introduction

Nuclear Medicine analyzes dynamic data of functional processes related to a specific metabolic activity. Nuclear medicine imaging data are acquired by means of devices that detect the product of the decay of radioisotopes in a radioactive tracer, which is bound to molecules with known biological properties and diffused in the living organism. Positron Emission Tomography (PET) [2, 27] is the most modern nuclear medicine

modality and FDG-PET is the PET modality in which the radiopharmaceutical [ $^{18}\text{F}$ ]-fluorodeoxyglucose (FDG) is used as a tracer to evaluate glucose metabolism [18]. FDG-PET dynamic images of tracer distribution, obtained from the measured radioactivity by applying an appropriate reconstruction algorithm, are a reliable estimate of the functional behaviour of glucose into tissues. Therefore, FDG-PET experiments allow clinicians to detect and stage diseases related to the pathological glucose consumption, such as cancer [1, 6, 40] or diabetes [3, 19].

Compartmental analysis [15, 33] is a powerful tool for processing dynamic PET data and estimating physiological kinetic parameters explaining the tracer metabolism. This kind of analysis relies on (I) the construction of a forward model (typically in the form of a Cauchy problem) for tracer concentration, in which the differential equations' coefficients are the kinetic parameters, and on (II) the application of an inversion technique to retrieve such kinetic parameters from measurements of the dynamic tracer concentration.

Compartmental analysis can be mainly subdivided in two classes: Regions Of Interest (ROI) kinetic modeling and parametric imaging. ROI-based methods [8, 11, 12, 39] return a single set of kinetic parameters for a homogeneous region of tissue, whose Time Activity Curve (TAC) is obtained averaging the PET activity over the region at each time frame. On the other hand, parametric imaging aims at evaluating the set of kinetic parameters for every pixel of the PET images, thus providing the spatial distribution of each model parameter. Recently, there has been increasing interest in the estimation of parametric images; this approach is particularly useful when the tissue under examination cannot be effectively segmented into homogeneous regions that could be modeled with a single kinetic parameter set. There exist *indirect* and *direct* approaches to parametric imaging. Indirect methods work by first reconstructing the dynamic PET images and then estimating the kinetic parameters at each pixel [44, 45]. Direct methods estimate directly the space-varying kinetic parameters from the measured PET sinogram [37]. The direct approach has been proved to reduce the Signal to Noise Ratio (SNR) with respect to indirect techniques [28], although strongly relies on the implementation of an efficient inversion algorithm capable of reconstructing the parameters on a dense set of pixels [17]. However, most parametric imaging methods (both direct and indirect) rely on linearized compartmental models and/or provide parametric images of algebraic combinations of the kinetic coefficients [22, 23, 29, 36, 38]. Rather few methods are able to reconstruct maps of each single parameter, and most of them consider simple one- and two-compartment models [7, 16, 17, 21].

Not many attempts have been devoted to the integration of the advances in the ROI-based compartmental modeling [41] in a parametric framework. In this paper, we introduce a new approach to indirect parametric imaging which is general enough to work for both two- and three-compartment models, effective enough to provide maps of all the kinetic coefficients involved, and that can be in principle integrated in a direct parametric imaging setting. This approach is based on a recently introduced ROI-based framework for the renal system [11] and extends it to determine parametric

mapping of such physiology. Further, the method can be in principle applied to a more general compartmental model (as done in the ROI-based framework in [10]), although in that case some more sophisticated implementation need to be applied to reduce the computational burden of parametric imaging.

The scheme of the paper is as follows. In Section 2 the two-compartment and three-compartment models are presented and the related forward problems are described. Section 3 deals with the formalization of the respective inverse problems and with the discussion of identifiability of the models. Section 4 describes the computational parametric imaging method. Section 5 provides the numerical validation of the computational method in the case of the two-compartment catenary model and then applies the method against experimental murine data for the analysis of the three-compartment non-catenary model of the renal system. Our conclusions are offered in Section 6.

## 2. Mathematical models

Compartmental analysis [15, 33] identifies different functional compartments in the physiological system of interest, each one associated with a specific metabolic state of the tracer. The tracer typically is injected into the blood and the tracer concentration in the blood is mathematically modeled by the so-called Input Function (IF) of the compartmental system. The time dependent concentrations of tracer in each compartment constitute the state variables of the model and can be determined from PET data. The time evolution of the state variables, i.e. the kinetics of the system, is here modeled by a linear system of Ordinary Differential Equations (ODEs) with constant coefficients, expressing the conservation of tracer during the flow between compartments. The coefficients define the input/output rate of tracer for each compartment and represent the physiological parameters describing the metabolism of the system. The forward problem is constructed by assuming that the tracer coefficients are known and by solving the ODE system for the unknown concentrations. We are aware that recent works [30] take into account macroscopic flow conditions (especially to model cardiac perfusion), introducing a PDE-based framework. However, the simplifying assumptions of time independence of parameters and of no spatial exchange between compartments are well established for FDG-PET analysis [42], and are the conditions assumed to hold throughout this paper.

This section is devoted to the description of the standard two-compartment catenary model and a three-compartment non-catenary model developed for the renal physiology and to the discussion of the related forward problems. In the following analysis, we denote with capital  $C$  (kBq ml<sup>-1</sup>) the concentrations and with the related suffixes the corresponding compartment; we use the notation  $k_{ij}$  (min<sup>-1</sup>) for the kinetic parameter describing the tracer exchange to the target compartment  $i$  from the source compartment  $j$ . The kinetic parameters (also known as rate constants or exchange coefficients) are real positive numbers and the plus or minus signs against

them characterize incoming and outgoing fluxes, respectively.

### 2.1. Two-compartment catenary system

The compartmental model describing the FDG metabolism of phosphorylation–dephosphorylation is the two-compartment catenary model shown in Figure 1 [9, 31].

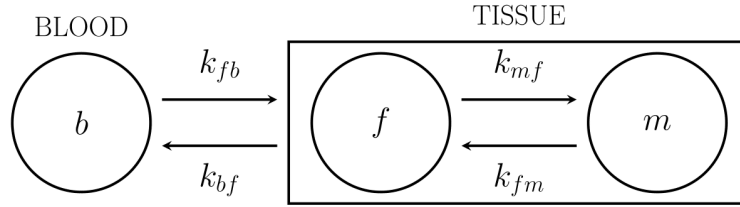


**Figure 1.** The compartmental model for the two-compartment catenary system describing the FDG metabolization in a generic tissue.

The two-compartment catenary model consists of:

- the blood compartment  $b$ ;
- two functional compartments: compartment  $f$ , accounting for free FDG, and compartment  $m$ , accounting for metabolized FDG;
- four exchange coefficients:  $k_{fb}$  and  $k_{bf}$  between the blood and the free compartment,  $k_{mf}$  and  $k_{fm}$  between the free and the metabolized ones.

Balance of tracer concentrations leads to the following multidimensional Cauchy problem:

$$\begin{cases} \dot{\mathbf{C}}(t) = \mathbf{M}\mathbf{C}(t) + \mathbf{w}(t) \\ \mathbf{C}(0) = \mathbf{0} \end{cases} \quad (1)$$

where

$$\mathbf{C} = \begin{pmatrix} C_f \\ C_m \end{pmatrix}, \quad \mathbf{M} = \begin{pmatrix} -(k_{bf} + k_{mf}) & k_{fm} \\ k_{mf} & -k_{fm} \end{pmatrix},$$

$$\mathbf{w} = k_{fb}C_b\mathbf{e}_1 = \begin{pmatrix} k_{fb}C_b \\ 0 \end{pmatrix} \text{ and } \mathbf{e}_1 = \begin{pmatrix} 1 \\ 0 \end{pmatrix}.$$

The analytical solution  $\mathbf{C}(t)$  of (1), formally expressing the forward problem of evaluating the concentrations from the kinetic parameters  $\mathbf{k} = (k_{fb}, k_{bf}, k_{mf}, k_{fm})^T$ , is given by

$$\mathbf{C}(t) = \int_0^t e^{(t-\tau)\mathbf{M}} \mathbf{w}(\tau) d\tau = k_{fb} \int_0^t e^{(t-\tau)\mathbf{M}} C_b(\tau) \mathbf{e}_1 d\tau, \quad t \in \mathbb{R}_+. \quad (2)$$

### 2.2. Three-compartment non-catenary system

Once injected into the system, the tracer reaches the kidneys and infuses the organs via the blood stream through the renal artery ( $a$ ), in Figure 2. Here, we

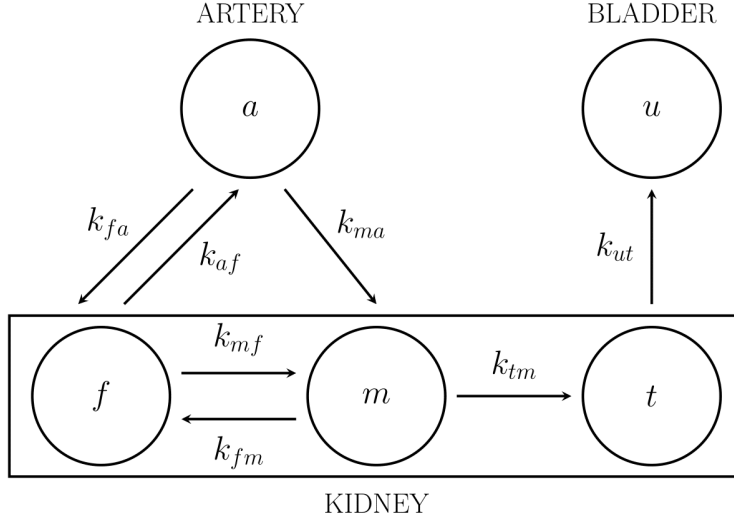


**Figure 2.** The compartmental model for the three-compartment non-catenary system describing the FDG kinetic inside the kidney.

consider the usual two-compartment model describing the FDG phosphorylation-dephosphorylation processes, obtaining the free tracer ( $f$ ) and the metabolized tracer ( $m$ ), both located in the extravascular kidney tissue. However, in order to study the role of the mechanisms transporting glucose back to the metabolism, we need to include the reabsorption compartment ( $t$ ), anatomically identified with the renal tubule. Moreover, we add the external urine compartment  $u$ , anatomically identified with the bladder, accounting for the tracer there accumulated, thanks to the excretion mechanism (differently from glucose, FDG is poorly absorbed in the renal tubule and is largely excreted in the urine, with accumulation in the bladder [35]).

The resulting three-compartment non-catenary model represented in Figure 2 [11] has the following kinetic parameters:

- $k_{fa}$  and  $k_{af}$  between the arterial IF and the free FDG compartment;
- $k_{ma}$  from the arterial compartment to the metabolized FDG one (filtration process);
- $k_{fm}$  and  $k_{mf}$  between the free FDG and the metabolized FDG compartments (phosphorylation and de-phosphorylation processes);
- $k_{tm}$  from the metabolized FDG compartment to the tubule (reabsorption process);
- $k_{ut}$  from the tubule compartment to the bladder pool (excretion process).

The resulting system of ODEs is:

$$\begin{cases} \dot{\mathbf{C}}(t) = \mathbf{M}\mathbf{C}(t) + \mathbf{w}(t) \\ \mathbf{C}(0) = \mathbf{0} \end{cases} \quad (3)$$

where

$$\mathbf{C} = \begin{pmatrix} C_f \\ C_m \\ C_t \end{pmatrix}, \quad \mathbf{M} = \begin{pmatrix} -(k_{af} + k_{mf}) & k_{fm} & 0 \\ k_{mf} & -(k_{fm} + k_{tm}) & 0 \\ 0 & k_{tm} & -k_{ut} \end{pmatrix},$$

$$\mathbf{w} = k_{fa}C_a\mathbf{e}_1 + k_{ma}C_a\mathbf{e}_2 = \begin{pmatrix} k_{fa}C_a \\ k_{ma}C_a \\ 0 \end{pmatrix}, \text{ and } \mathbf{e}_1 = \begin{pmatrix} 1 \\ 0 \\ 0 \end{pmatrix} \text{ and } \mathbf{e}_2 = \begin{pmatrix} 0 \\ 1 \\ 0 \end{pmatrix}.$$

The analytical solution for  $\mathbf{C}$ , in terms of the kinetic coefficients  $\mathbf{k} = (k_{fa}, k_{ma}, k_{af}, k_{mf}, k_{fm}, k_{tm}, k_{ut})^T$ , is given by

$$\mathbf{C}(t) = \int_0^t e^{(t-\tau)\mathbf{M}}\mathbf{w}(\tau) d\tau = \quad (4)$$

$$= k_{fa} \int_0^t e^{(t-\tau)\mathbf{M}}C_a(\tau)\mathbf{e}_1 d\tau + k_{ma} \int_0^t e^{(t-\tau)\mathbf{M}}C_a(\tau)\mathbf{e}_2 d\tau, \quad t \in \mathbb{R}_+. \quad (5)$$

The bladder compartment is the only compartment whose volume changes (specifically increases) in time. This condition is expressed by equation

$$\frac{d}{dt}(V_u C_u) = F_{ut} C_t \quad \text{with} \quad C_u(0) = 0, \quad (6)$$

where  $V_u$  indicates the bladder volume and  $F_{ut}$  the bulk flow entering the bladder from the tubule.

### 3. Inverse problem: data and solution

The forward model equation, as the analytical solution to the system of ODEs, describes the time behavior of the tracer concentration given the TAC for tracer concentration in blood and the exchange coefficients. Given such equation, compartmental analysis requires the determination of the parameters by utilizing measurements of the tracer concentrations provided by PET imaging and applying an optimization scheme for the solution of the inverse problem. The reconstructed PET images of tracer concentration supply information on the IF and provide an estimate of the sum of the concentrations of the different compartments considered, at each time point of the acquisition. In this work, we make use of the Gauss-Newton method [4], supplied with a regularizing term, to estimate the exchange parameters.

Let us denote by  $\tilde{C}$  the PET experimental concentration in a specific tissue (either a ROI or a single pixel) and by  $C_b$  the IF. Consider a compartmental model with  $m$  compartments  $1, \dots, m$  and an arbitrary number  $p$  of exchange coefficients  $k_1, \dots, k_p$ . Then  $\tilde{C}$  can be expressed as

$$\tilde{C}(t) = \sum_{i=1}^m C_i(t) \quad \forall t \in \mathbb{R}_+. \quad (7)$$

Equivalently, we can write

$$\tilde{C}(t) = \boldsymbol{\alpha}^T \mathbf{C}(t), \quad (8)$$

where

$$\boldsymbol{\alpha} = \begin{pmatrix} 1 \\ 1 \\ \vdots \\ 1 \end{pmatrix} \quad \text{and} \quad \mathbf{C} = \begin{pmatrix} C_1 \\ C_2 \\ \vdots \\ C_m \end{pmatrix}$$

and where we assembled the available experimental data at the left-hand side. In particular, the inverse problem equations for the two compartmental models considered in this paper are the following.

- Two-compartment catenary system:

$$\tilde{C}(t) = \boldsymbol{\alpha}^T \mathbf{C}(t) \text{ with } \boldsymbol{\alpha} = \begin{pmatrix} 1 \\ 1 \end{pmatrix} \text{ and } \mathbf{C} = \begin{pmatrix} C_f \\ C_m \end{pmatrix}, \quad (9)$$

where  $\mathbf{C}$  is given by equation (2).

- Three-compartment non-catenary system:

$$\tilde{C}(t) = \boldsymbol{\alpha}^T \mathbf{C}(t) \text{ with } \boldsymbol{\alpha} = \begin{pmatrix} 1 \\ 1 \\ 1 \end{pmatrix} \text{ and } \mathbf{C} = \begin{pmatrix} C_f \\ C_m \\ C_t \end{pmatrix}, \quad (10)$$

where  $\mathbf{C}$  is given by equation (5).

We re-write equation (8) for the unknown vector parameter  $\mathbf{k} = (k_1, \dots, k_p)$  in the form

$$\tilde{C}(t) - \boldsymbol{\alpha}^T \mathbf{C}(t) := \mathcal{F}_t(\mathbf{k}) = 0 \quad \forall t \in \mathbb{R}_+, \quad (11)$$

where  $\mathcal{F}_t: \mathbb{R}_+^p \rightarrow C^1(\mathbb{R}_+, \mathbb{R}_+)$  is a non-linear operator parameterized by the time variable  $t \in \mathbb{R}_+$ . We then have to deal with a non-linear zero-finding problem, which is solved following the procedure used in [10] by means of a Gauss-Newton method with a regularizing term accounting for the ill-posedness of the problem. The Gauss-Newton approach transforms the non-linear optimization problem of finding the exchange coefficients into a linear problem by computing the Fréchet derivative of equation (11) with respect to the exchange coefficients. The optimization algorithm performs an iterative scheme, which increases the value of the  $i$ -th approximation of  $\mathbf{k}$  by a step-size determined solving a regularized least-squares problem.

### 3.1. Uniqueness theorems

The identifiability analysis [26, 43] of compartmental models is a necessary step in the solution process, since the uniqueness of the reconstructed parameters is an essential property which makes the model effective in the description of the physiological processes under investigation.

As shown in [9], the two-compartment catenary systems describing the FDG cellular metabolism is always identifiable, i.e. the following theorem holds.

**Theorem 3.1.** *The inverse problem for the two-compartment catenary system of equation (9) has a unique solution  $\mathbf{k} = (k_{fb}, k_{bf}, k_{mf}, k_{fm})^T \in \mathbb{R}_+^{4*}$  determined from the PET experimental measurements  $C_b$  and  $\tilde{C}$ .*

We show here that the three-compartment non-catenary model for the renal system is also identifiable, by exploiting the conditions established by the renal physiology.

**Theorem 3.2.** *By assuming that the polynomials*

$$P(s) = k_{ma}(s + k_{af} + k_{mf}) + k_{fa}k_{mf}$$

*and*

$$Q(s) = k_{fa}(s + k_{fm} + k_{tm}) + k_{ma}k_{fm}$$

*are both coprime with the polynomial*

$$D(s) = (s + k_{af} + k_{mf})(s + k_{fm} + k_{tm}) - k_{mf}k_{fm} ,$$

*the inverse problem for the three-compartment non-catenary system of equation (10) has a unique solution  $\mathbf{k} = (k_{fa}, k_{ma}, k_{af}, k_{mf}, k_{fm}, k_{tm}, k_{ut})^T \in \mathbb{R}_+^{7*}$  determined from the PET experimental measurements  $C_a$  and  $\tilde{C}$ .*

*Proof.* We remark some physiological considerations.

- (i) Under the assumption of stationarity, the growth of the bladder volume  $V_u$  during time can be considered as linear [11]:

$$F_{ut} = \frac{V_u(t_f) - V_u(\bar{t})}{t_f - \bar{t}} , \quad (12)$$

where  $t_f$  is the ended time point and  $\bar{t}$  is a generic time instant. Thus, from experimental values of  $V_u$  at different time points we obtain an estimate of  $F_{ut}$ .

- (ii) Physiological considerations lead to [25]

$$F_{tm} = 10^2 F_{ut} , \quad (13)$$

where  $F_{tm}$  is the bulk flow entering in the renal tubule.

- (iii) The balance of tracer flow inside the tubule is given by [11]

$$\frac{d}{dt}(V_K V_t C_t) = F_{tm} C_m - F_{ut} C_t , \quad (14)$$

where  $V_K$  is the renal volume,  $V_t$  the fraction of the tubule volume, and thus  $V_K V_t$  is the total volume of the tubule.

The third differential equation of the ODE system (3) accounts for the dynamic of the tubule compartment concentration:

$$\frac{d}{dt}C_t = \dot{C}_t = k_{tm}C_m - k_{ut}C_t . \quad (15)$$

Comparing (14) and (15), we get

$$k_{tm} = \frac{F_{tm}}{V_K V_t} := \alpha \quad k_{ut} = \frac{F_{ut}}{V_K V_t} := \beta , \quad (16)$$

that are given from physiological experimental data. Moreover, equations (13) and (16) imply the physiological condition  $k_{tm} = 10^2 k_{ut}$ .

There are still five unknown exchange coefficients to be determined, in the sequel denoted by

$$k_{fa} = a , \quad k_{ma} = b , \quad k_{af} = c , \quad k_{mf} = d , \quad k_{fm} = e .$$



Therefore, the ODE system (3) takes the form

$$\begin{cases} \dot{C}_f = -(c+d)C_f + eC_m + aC_a \\ \dot{C}_m = dC_f - (e+\alpha)C_m + bC_a \\ \dot{C}_t = \alpha C_m - \beta C_t . \end{cases} \quad (17)$$

Assuming that the concentrations are sufficiently regular, we take the Laplace transform of the differential equations (17) (for the three compartments inside the kidney) and of equation (6) (for the bladder compartment):

$$(s+c+d)\mathcal{L}(C_f) - e\mathcal{L}(C_m) = a\mathcal{L}(C_a) \quad (18a)$$

$$-d\mathcal{L}(C_f) + (s+e+\alpha)\mathcal{L}(C_m) = b\mathcal{L}(C_a) \quad (18b)$$

$$\alpha\mathcal{L}(C_m) = (s+\beta)\mathcal{L}(C_t) \quad (18c)$$

$$s\mathcal{L}(V_u C_u) = F_{ut}\mathcal{L}(C_t) , \quad (18d)$$

where  $\mathcal{L}(f)$  denotes the Laplace transform of the function  $f$ . Solving the subsystem of equations (18a–18b) with respect to  $C_f$  and  $C_m$ , we get

$$\mathcal{L}(C_f) = \frac{a(s+e+\alpha) + be}{D} \mathcal{L}(C_a) \quad (19a)$$

$$\mathcal{L}(C_m) = \frac{b(s+c+d) + ad}{D} \mathcal{L}(C_a) \quad (19b)$$

where  $D = (s+c+d)(s+e+\alpha) - de$ . Solving the subsystem of equation (18c–18d) with respect to  $C_t$ , we get

$$\mathcal{L}(C_t) = \frac{\alpha}{s+\beta} \mathcal{L}(C_m) = \frac{\alpha}{s+\beta} \frac{b(s+c+d) + ad}{D} \mathcal{L}(C_a) \quad (20a)$$

$$\mathcal{L}(C_t) = \frac{s\mathcal{L}(V_u C_u)}{F_{ut}} , \quad (20b)$$

from which we have

$$\frac{s+\beta}{\alpha} \frac{s\mathcal{L}(V_u C_u)}{F_{ut}\mathcal{L}(C_a)} = \frac{b(s+c+d) + ad}{D} . \quad (21)$$

The left-hand side is a function of the variable  $s$  depending only on the known experimental data and the right-hand side is a polynomial fraction in  $s$  depending on the unknown coefficients. Therefore,  $\mathcal{L}(C_m)$  (by comparing (19b) and (21)) and  $\mathcal{L}(C_t)$  are functions of  $s$  independent from the unknown parameters. Then, we apply the Laplace transform to equation (10) for the kidney system and we obtain

$$\mathcal{L}(\tilde{C}) - \mathcal{L}(C_m) - \mathcal{L}(C_t) = \mathcal{L}(C_f) , \quad (22)$$

where the left-hand side is a known function of  $s$  involving only known factors, while the right-hand side is a polynomial fraction in  $s$  as in (19a).

Now, suppose  $(a', b', c', d', e')$  is an alternative choice of rate coefficients consistent with the data of the problem. Thus, the left-hand side of equations (21) and (22) is

necessarily equal for the two sets of parameters; therefore, we get

$$\frac{b(s + c + d) + ad}{D} = \frac{b'(s + c' + d') + a'd'}{D'} \quad (23)$$

$$\frac{a(s + e + \alpha) + be}{D} = \frac{a'(s + e' + \alpha) + b'e'}{D'} , \quad (24)$$

where  $D' = (s + c' + d')(s + e' + \alpha) - d'e'$ . Assuming that the two rational fractions (23) and (24) are irreducible, i.e. the polynomials  $P(s) = b(s + c + d) + ad$  and  $Q(s) = a(s + e + \alpha) + be$  are both coprime with  $D(s)$ , we obtain the relationships between the first and the second set of parameters, i.e. the system

$$\begin{cases} b = b' \\ (c + d) + ad = b'(c' + d') + a'd' \\ c + d + e + \alpha = c' + d' + e' + \alpha \\ e + (c + d)\alpha = c'e' + (c' + d')\alpha \\ a = a' \\ a(e + \alpha) + be = a'(e' + \alpha) + b'e' \end{cases} ,$$

which holds if and only if

$$a = a' , \ b = b' , \ c = c' , \ d = d' , \ e = e' .$$

□

#### 4. The imaging method

In this section we present a parametric imaging method, which relies upon the application of image processing algorithms and of a rather general optimization scheme based on the regularized Gauss-Newton method [10] able to solve the compartmental inverse problem pixelwise. We remark that our method is potentially applicable to any generic compartmental model, provided an 'ad hoc' identifiability study and taking into account the compartment-dependent increase of the computational cost.

We start from the set of  $N$  reconstructed dynamic FDG-PET images:

$$(\mathbf{f}_1^{(t)}, \mathbf{f}_2^{(t)}, \dots, \mathbf{f}_N^{(t)}) \text{ for } t = 1, \dots, T , \quad (25)$$

where  $\mathbf{f}_n^{(t)}$  is the  $n$ -th PET image at  $t$ -th time point of tracer concentration  $\tilde{C}$ , i.e.

$$\mathbf{f}_n^{(t)}(i, j) = \tilde{C}_{(i,j)}(t) \text{ for } i = 1, \dots, I, \ j = 1, \dots, J , \quad (26)$$

and  $I, J$  are the image dimensions.

We select the tissue of interest and the compartmental model reliable for its functional description. For each dynamic PET image  $(\mathbf{f}_{\bar{n}}^{(1)}, \dots, \mathbf{f}_{\bar{n}}^{(T)})$ ,  $\bar{n} \in \{1, \dots, N\}$ , i.e. a PET slice, our imaging method follows the steps described below.

**Step 1. Gaussian smoothing.** In order to reduce the noise due to data acquisition, we apply a Gaussian smoothing filter through the convolution operation

$$\tilde{\mathbf{f}}_{\bar{n}}^{(t)} = \mathbf{f}_{\bar{n}}^{(t)} * \mathbf{G}_{0,\sigma} \ \forall t = 1, \dots, T , \quad (27)$$

where

$$\mathbf{G}_{0,\sigma}(i, j) = \frac{1}{2\pi\sigma^2} e^{-\frac{\mathbf{x}(i,j)^2 + \mathbf{y}(i,j)^2}{2\sigma^2}} \text{ and} \quad (28)$$

$$\mathbf{x}(i, j), \mathbf{y}(i, j) \in \left\{-\frac{L-1}{2}, \dots, \frac{L-1}{2}\right\} \times \left\{-\frac{L-1}{2}, \dots, \frac{L-1}{2}\right\}, \quad (29)$$

and  $L$  is the (odd) dimension of the window. In all our applications, we use a Gaussian convolution matrix  $\mathbf{G}_{0,\sigma}$  with zero mean, standard deviation  $\sigma = 1$  and dimension  $L = 3$ .

**Step 2. Image segmentation.** To extract the ROI  $\mathbf{A}$ , which delimits the organ of physiologic interest, we apply the following image segmentation method:

- (i) compute the PET image averaged in time:  $\tilde{\mathbf{f}}_{\bar{n}} = \frac{1}{T} \sum_{t=1}^T \tilde{\mathbf{f}}_{\bar{n}}^{(t)}$ ;
- (ii) consider the pixel with maximum intensity  $(\bar{i}, \bar{j}) = \max_{i,j} \tilde{\mathbf{f}}_{\bar{n}}(i, j)$ ;
- (iii) approximate the profile of the  $\bar{i}$ -th matrix row with a family of one-dimensional Gaussian functions of variable variance, by means of a curve fitting process. This consists in computing

$$\bar{\sigma} = \arg \min_{\sigma} \|\tilde{\mathbf{f}}_{\bar{n}}(\bar{i}, j) - G_{\bar{j},\sigma}(j)\|; \quad (30)$$

- (iv) determine the activity's lower bound in the ROI as the value  $\bar{c}$  at which the two curves  $\tilde{\mathbf{f}}_{\bar{n}}(\bar{i}, j)$  and  $G_{\bar{j},\bar{\sigma}}(j)$  separate from each other. The ROI encompassing the organ is thus defined as

$$\mathbf{A}(i, j) = \begin{cases} 0 & \text{if } \tilde{\mathbf{f}}_{\bar{n}}(i, j) < \bar{c} \\ 1 & \text{if } \tilde{\mathbf{f}}_{\bar{n}}(i, j) \geq \bar{c} \end{cases}. \quad (31)$$

We model the outer region of the organ of interest with a standard two-compartment model; the ROI  $\mathbf{A}$  is described by the most reliable compartmental model (according to the organ physiology).

**Step 3. Parameter estimation.** We apply the regularized Gauss-Newton algorithm [10] pixelwise, following the idea presented in Section 3. In general, for a compartmental model with  $p$  arbitrary kinetic parameters, for each image pixel  $(i, j) \in \{1, \dots, I\} \times \{1, \dots, J\}$ , the reconstruction iterative algorithm is:

- (i) choose the initial guess:  $\mathbf{k}_{(i,j)}^{(0)} \in \mathbb{R}_+^p$ ;
- (ii) solve for  $\boldsymbol{\delta}_{(i,j)}^{(0)} \in \mathbb{R}^p$

$$(r^{(0)} \mathbf{I} + \mathbf{F}^{(0)T} \mathbf{F}^{(0)}) \boldsymbol{\delta}_{(i,j)}^{(0)} = \mathbf{F}^{(0)T} (\tilde{C}_{(i,j)}(t) - \boldsymbol{\alpha}^T \mathbf{C}_{(i,j)}^{(0)}(t)), \quad (32)$$

where  $\mathbf{F}^{(0)}$  encodes the Fréchet derivatives with respect to the exchange coefficients,  $\tilde{C}_{(i,j)}(t)$  is the measured PET experimental concentration at  $(i, j)$ ,  $\mathbf{C}_{(i,j)}^{(0)}$  is the vector of concentrations predicted according to the model and  $r^{(0)}$  is the regularization parameter optimized through the Generalized Cross Validation (GCV) method [14];

- (iii) update  $\mathbf{k}_{(i,j)}^{(0)}$  with step-size  $\boldsymbol{\delta}_{(i,j)}^{(0)}$ :

$$\mathbf{k}_{(i,j)}^{(1)} = \mathbf{k}_{(i,j)}^{(0)} + \boldsymbol{\delta}_{(i,j)}^{(0)}, \quad (33)$$

and iterate.

To stop the iterative algorithm we check the discrepancy between the experimental dynamic concentration and the predicted one, using a threshold of the order of  $10^{-2}$  as a stopping criterion.

**Step 4. Parametric images.** Once we obtain the set of exchange coefficients of the model for each image pixel, we build up the parametric images  $\mathbf{K}_1, \dots, \mathbf{K}_p$ :

$$\mathbf{K}_1(i, j) = \mathbf{k}_{(i,j)}(1), \dots, \mathbf{K}_p(i, j) = \mathbf{k}_{(i,j)}(p) . \quad (34)$$

Regarding Step 1. and Step 2., other imaging processing methods can be used to smooth and segment PET images; the impact of other approaches on the accuracy of compartmental analysis is under investigation. However, simple gaussian smoothing, as in Step 1., and our *ad hoc* image segmentation process, as in Step 2., provide good results regardless of the not high resolution of PET images involved in the analysis.

## 5. Numerical applications

Our new parametric imaging method is here applied against both synthetic and real microPET data of murine models [20, 32]. In particular, we test the procedure with the two-compartment model in the simulation framework and with the three-compartment model, describing the renal system, in the real data framework.

### 5.1. Simulation

Synthetic data are created mimicking a real FDG-microPET acquisition: first we choose a phantom (as in Figure 3(a)) encompassing four homogeneous regions; for every region, a set of realistic kinetic parameters of a two-compartmental problem is assigned as ground truth (Table 1). Therefore, we obtain four synthetic parametric images  $\mathbf{K}_1, \mathbf{K}_2, \mathbf{K}_3, \mathbf{K}_4$ , each one characterized by a specific set of kinetic parameters. The ground truth parametric images are displayed in Figure 4.

**Table 1.** Ground truth numerical values of the kinetic parameters for each one of the four regions.

	$k_1$	$k_2$	$k_3$	$k_4$
region 1	0.8	0.6	0.07	0.07
region 2	1	1	0.2	0.2
region 3	1.1	0.9	0.5	0.4
region 4	0.5	0.5	0.1	0.01

The dynamic PET images of tracer concentration are generated solving pixelwise the forward compartmental problem (1–2), according to the following scheme:

- (i) compute the values of the integral (2) using the ground truth values of the parameters and a simulated blood IF (Figure 3(b)), obtained by fitting with a

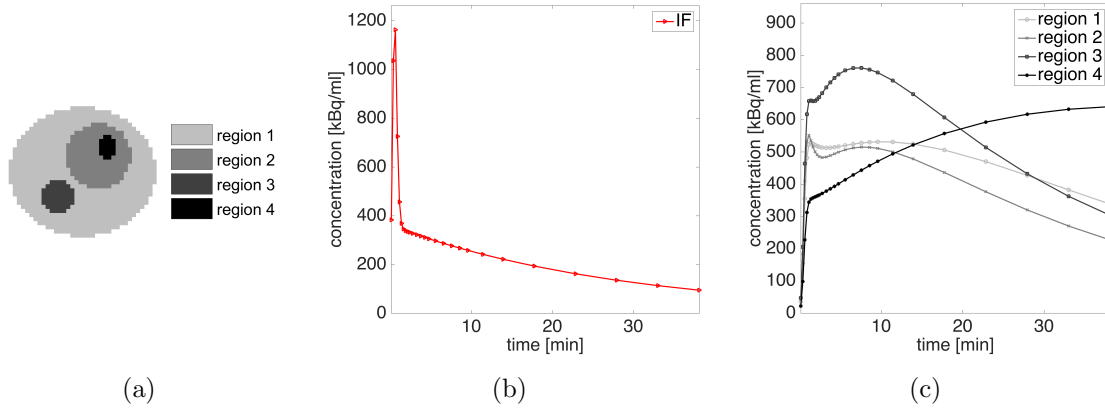


**Figure 3.** The FDG-PET simulation setting. (a) Phantom composed by four homogeneous regions. (b) The simulated blood IF. (c) The characteristic TAC for each region.

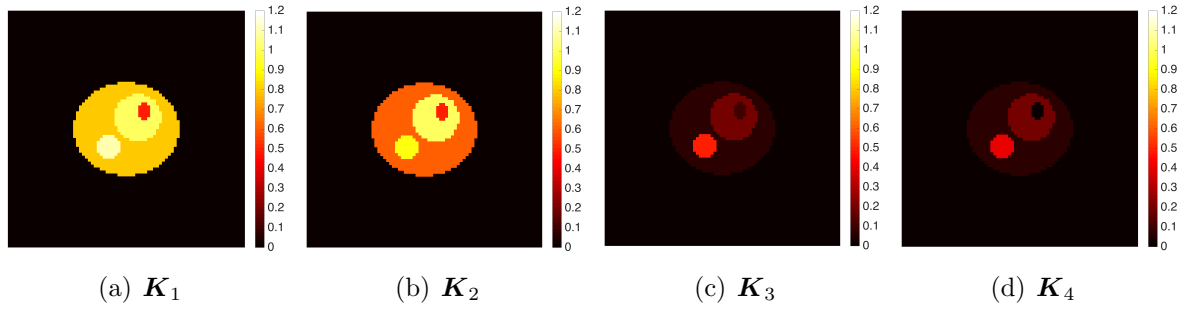


**Figure 4.** The ground truth parametric images  $K_1, K_2, K_3, K_4$  of the two-compartment system.

gamma variate function [13] a set of real measurements acquired from a healthy mouse in a very controlled experiment;

- (ii) evaluate the synthetic FDG-microPET concentration by means of equation (9);
- (iii) sample on time interval  $[t_1; t_N]$  of 27 time frames equivalent to the typical total acquisition time of the FDG experiments performed with the microPET scanner available at our lab (Albira, Carestream Health, Genova) and in agreement with usual time points of the experiments ( $10 \times 15s$ ,  $1 \times 22s$ ,  $4 \times 30s$ ,  $5 \times 60s$ ,  $2 \times 150s$  and  $5 \times 300s$ ).

Characteristic TACs of each region are shown in Figure 3(c). Finally, we affect the synthetic dynamic concentrations with Poisson noise, i.e. the counting noise typical of nuclear medicine data, to simulate the experimental conditions and we create fifty independent identically-distributed noisy datasets.

For each dataset, we follow the reconstruction steps of Section 4, i.e. we apply the Gaussian smoothing filter ( $\sigma = 1$ , window  $3 \times 3$ ) on the dynamic PET images and solve pixelwise the compartmental inverse problem by means of the regularized Gauss-Newton algorithm. For each pixel, the starting point of our method is randomly chosen in the

interval  $(0, 1)$  and the regularization parameter is optimized at each iteration through the GCV method. We do not need to apply the image segmentation step because in this simulation we model the same two-compartment scheme for all the pixels.

Once the entire set of kinetic parameters  $k_1, k_2, k_3, k_4$  for each pixel are retrieved, we build up the parametric images  $\mathbf{K}_1, \mathbf{K}_2, \mathbf{K}_3, \mathbf{K}_4$ . Figure 5 shows the mean images (first row) and the standard deviation images (second row), computed over the fifty reconstructions. The mean images provide a reliable approximation of the ground truth parametric images, demonstrating the consistency of the parametric inversion procedure. The standard deviation images keep systematically small values, proving that the iterative reconstruction scheme is numerically stable with respect to noise. Table 2 reports the mean and the standard deviation of the kinetic parameters over the four homogeneous regions. Comparison between the ground truth values of Table 1 and the reconstructed values of Table 2 clearly shows the reliability of our approach.

From the computational viewpoint, the parametric reconstruction takes almost 45 minutes. Please note that the algorithm was implemented in the Matlab programming environment and the algorithm was executed on a computer with a processor Intel core i5. Despite that, for a single pixel, the Gauss-Newton iterative scheme requires about 5-10 iterations before it converges and the operations carried out in a single iteration for computing the Newton step-size are not computationally demanding (the matrices in the game have small size). Therefore, the high computational cost of the method depends only from the application of the reduction scheme on a dense set of pixels. Nevertheless, the computational complexity of our parametric imaging method is consistent with standard parametric methods.

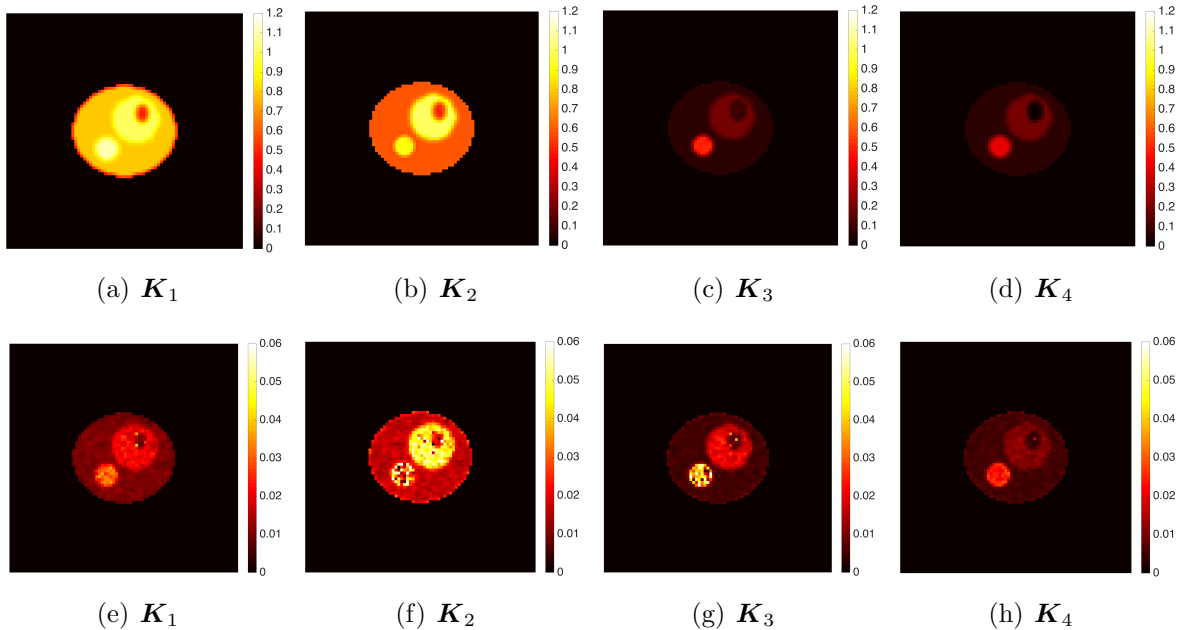


**Figure 5.** Mean images (first row) and standard deviation images (second row) of  $\mathbf{K}_1, \mathbf{K}_2, \mathbf{K}_3, \mathbf{K}_4$ , computed over the fifty reconstructions.

**Table 2.** Mean and standard deviation of the kinetic parameters for each homogeneous region, computed over the fifty reconstructions.

	$k_1$	$k_2$	$k_3$	$k_4$
region 1	$0.76 \pm 0.01$	$0.60 \pm 0.02$	$0.07 \pm 0.01$	$0.07 \pm 0.01$
region 2	$0.96 \pm 0.02$	$0.93 \pm 0.04$	$0.17 \pm 0.02$	$0.17 \pm 0.01$
region 3	$1.05 \pm 0.02$	$0.81 \pm 0.03$	$0.38 \pm 0.04$	$0.33 \pm 0.02$
region 4	$0.58 \pm 0.01$	$0.57 \pm 0.03$	$0.09 \pm 0.01$	$0.02 \pm 0.01$

### 5.2. Real data

We now test our parametric imaging method on real FDG-PET experiments in the case of the three-compartment non-catenary model representing the renal physiology, described in Subsection 2.2.

We analyzed FDG-PET real data of murine models obtained by means of the dedicated microPET system (Albira, Carestream Health, Genova) [5] currently operational at our lab. Following the experimental protocol for FDG-PET experiments, utilized during a study on the metabolic effects of metformin [24], the animals were studied after a fasting period of six hours to ensure a steady state of substrate and hormones governing glucose metabolism. Then, the animals were properly anesthetized and positioned on the bed of the microPET system whose two-ring configuration covers the whole animal body in a single bed position. A dose of 3 to 4 MBq of FDG was injected through the tail vein, soon after the start of a dynamic list mode acquisition lasting 40 min. The acquisition was reconstructed using the following framing rate:  $10 \times 15s$ ,  $1 \times 22s$ ,  $4 \times 30s$ ,  $5 \times 60s$ ,  $2 \times 150s$  and  $5 \times 300s$ . The dynamic PET images of tracer concentration (kBq/ml) were reconstructed using a Maximum Likelihood Expectation Maximization (MLEM) method [34]. The complete dataset is composed by 100 images of  $80 \times 80$  pixels, each one reproducing an axial section, by the total number of time points of the experiment. For this test, we considered a mouse in a control (CTR) condition and a mouse in a starved (STS) condition (food deprivation, with free access to water, for 48 hours). We focused on the analysis of the renal physiology and selected a single PET slice containing an axial section of the right kidney, the same slice for both animals. The entire FDG kinetic process was initialized by the arterial IF. We are aware that the determination of IF is a challenging task in the case of mice. To accomplish it, for each animal model we have first viewed the tracer pass in cine mode. Then, in a frame where the left ventricle was particularly visible, we have drawn a ROI in the aortic arc and maintained it for all time points.

We applied our imaging method on the selected dynamic PET slice of the CTR mouse and of the STS mouse. More specifically, we smoothed the data by means of a Gaussian filter of standard deviation  $\sigma = 1$  and size  $3 \times 3$ ; we selected the ROI within the axial section of the kidney through the image segmentation process determining the minimum value of activity recorded inside the organ, and reconstructed

the kinetic parameters  $k_{fa}, k_{ma}, k_{af}, k_{mf}, k_{fm}, k_{tm}, k_{ut}$  of the three-compartment system for each pixel by means of the regularized Gauss-Newton iterative algorithm. The initial guesses were randomly selected in the interval  $(0, 1)$  and the regularization parameter was chosen by the GCV method. The reconstructed parametric images  $\mathbf{K}_{fa}, \mathbf{K}_{ma}, \mathbf{K}_{af}, \mathbf{K}_{mf}, \mathbf{K}_{fm}, \mathbf{K}_{tm}, \mathbf{K}_{ut}$  for the renal compartmental model are presented in Figure 6 and Figure 7: in each figure, the first row shows the parametric images for the CTR mouse, the second row for the STS mouse.

All parametric images, of both the CTR mouse and the STS mouse, show parameters' values that vary quite largely from pixel to pixel, bringing out the lack of homogeneity of the renal tissue. Indeed, the parametric images point out the different structures composing the kidney and characterizing the distinct functions of the organ [25]. This is consistent with the architecture of the renal compartmental model we have designed (Subsection 2.2). The higher activity of the parameters is located in a specific part of the outer portion of the axial section of the kidney, which is attributable to the renal cortex, in which most of the renal processes are carried out. Moreover, for both the CTR and STS conditions, we can observe that the parametric images  $\mathbf{K}_{tm}$  and  $\mathbf{K}_{ut}$  linked to the tubule compartment have a very similar distribution while the physiologically sound condition  $k_{tm} \simeq 10^2 k_{ut}$  is maintained pixelwise (without any constraint in the inversion procedure). Instead, the fundamental difference between the CTR and the STS parametric images is the order of magnitude of the numerical values of the parameters. From the CTR mouse to the STS mouse, the values of the exchange coefficients associated with the blood input, that are  $k_{fa}, k_{ma}, k_{af}$ , decrease of two order of magnitudes, while the values of the parameters  $k_{tm}$  and  $k_{ut}$  decrease of one order of magnitude. This discrepancy reflects the response of the kidney to the different physiological conditions of the two mice analyzed, coherently with what already observed [11]. Finally, we notice that the parameters linked to the FDG metabolism process,  $k_{mf}$  and  $k_{fm}$ , remain unchanged in the two conditions.

## 6. Conclusions

FDG-PET imaging allows the observation of metabolic processes related to glucose consumption inside a living organism. In order to overcome the limits of spatial resolution in PET and to improve the quality of information achievable from PET images, one solution is to develop parametric imaging methods capable of showing the tracer metabolism at local level. Starting from the design of compartmental models suitable to describe the tracer kinetics in a predefined physiological system, parametric imaging techniques process dynamic PET images and estimate the spatial distribution of the exchange coefficients identified by the model.

In this paper we have shown a novel parametric imaging approach which solves pixelwise the non-linear compartmental inverse problem of retrieving the kinetic parameters from dynamic tracer concentration data by means of a Gauss-Newton algorithm with a penalty term accounting for the ill-posedness of the problem. The



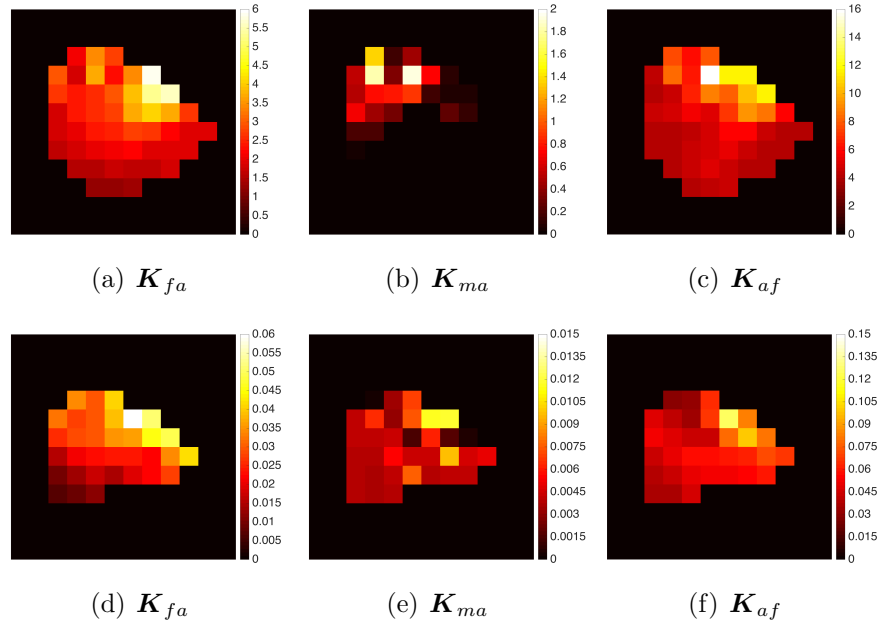


**Figure 6.** Parametric images  $K_{fa}, K_{ma}, K_{af}$ : first row for the CTR mouse, second row for the STS mouse.

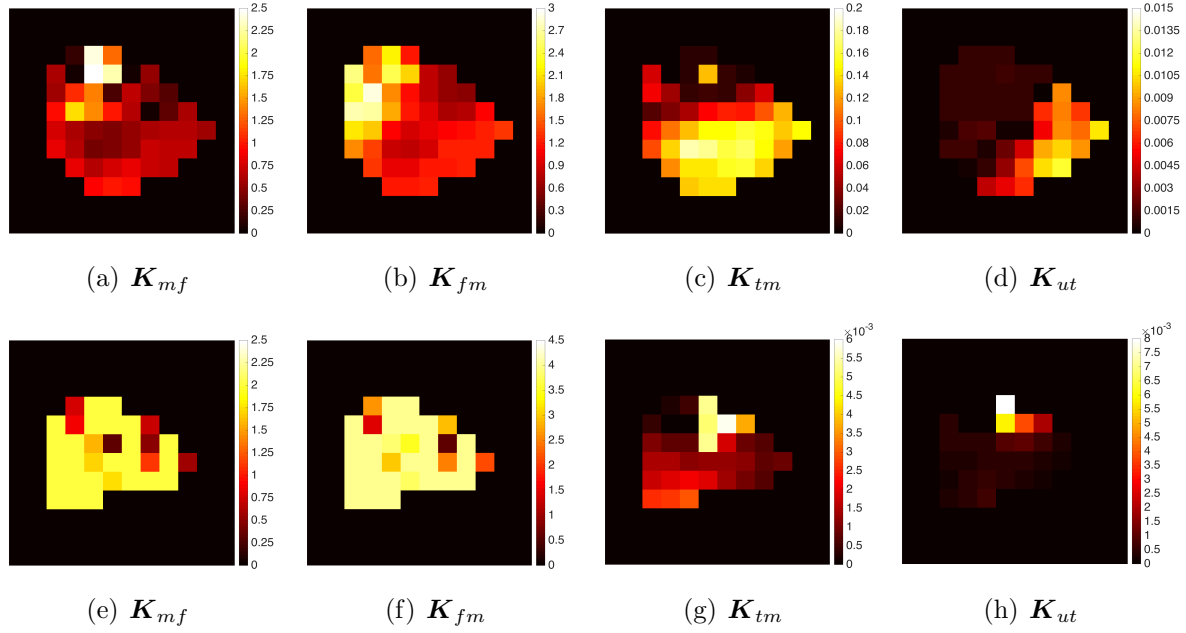


**Figure 7.** Parametric images  $K_{mf}, K_{fm}, K_{tm}, K_{ut}$ : first row for the CTR mouse, second row for the STS mouse.

main advantage of this approach is in its notable degree of generality, since in principle it may be applied to models made of several compartments. Further, differently to typical linear parametric imaging methods, this algorithm provides maps of all model parameters. We focused on the standard two-compartment catenary model and a three-compartment non-catenary model representing the renal system. However, we remark

that the procedure can be applied also for a large variety of compartmental models, more general and complicated, provided that the numerical complexity of the model is taken into account.

We validated our approach against synthetic data and then tested it on FDG-PET data of murine models. We analyzed dynamic FDG-PET images of a selected axial section of the right kidney for a control mouse and a starved mouse, proving that the reconstructed renal parametric images are qualitatively effective in the description of the local FDG metabolism.

Further developments of this approach to parametric images of nuclear medicine data are concerned with two issues. From the computational viewpoint, we aim at reducing the computational burden of this approach by means of 'ad hoc' designed implementations. From the clinical viewpoint, we are going to apply this approach against a notable quantity of data acquired according to paradigms designed to investigate the role of metformin in glucose metabolism [24].

## References

- [1] Annibaldi A and Widmann C 2010 Glucose metabolism in cancer cells *Curr. Opin. Clin. Nutr. Metab. Care* **13** 466–470
- [2] Bailey D, Townsend D, Valk P and Maisey M 2005 Positron Emission Tomography - Basic Sciences *Springer-Verlag London Limited*
- [3] Basu A, Basu R, Shah P, Vella A, Johnson C, Nair K, Jensen M, Schwenk W and Rizza R 2000 Effects of type 2 diabetes on the ability of insulin and glucose to regulate splanchnic and muscle glucose metabolism: evidence for a defect in hepatic glucokinase activity *Diabetes* **49** 272–283
- [4] Bauer F, Hohage T and Munk A 2009 Iteratively regularized Gauss–Newton method for nonlinear inverse problems with random noise *SIAM J. Numerical Analysis* **47** 1827–1846
- [5] Bruker 2012 Albira Imaging *Bruker Albira Imaging System User Manual*
- [6] Cairns R A, Harris I S and Mak T W 2011 Regulation of cancer cell metabolism *Nat. Rev. Cancer* **11** 85–95
- [7] Carson R E and Lange K 1985 The EM parametric image reconstruction algorithm *J. Am. Stat. Assoc.* **80** 20–22
- [8] Carson R E 2003 Tracer Kinetic Modeling in PET *Springer-Verlag London Limited* 147–179.
- [9] Delbary F, Garbarino S and Vivaldi V 2016 Compartmental analysis of dynamic nuclear medicine data: models and identifiability *Inverse Problems* **32** 125010
- [10] Delbary F and Garbarino S 2016 Compartmental analysis of dynamic nuclear medicine data: regularization procedure and application to physiology *ArXiv:1608.01825*
- [11] Garbarino S, Caviglia G, Sambuceti G, Benvenuto F and Piana M 2014 A novel description of FDG excretion in the renal system: application to metformin-treated models *Phys. Med. Biol.* **59** 2469–2484
- [12] Garbarino S, Vivaldi V, Delbary F, Caviglia G, Piana M, Marini C, Capitano S, Calamia I, Buschiazzi A, and Sambuceti G 2015 A new compartmental method for the analysis of liver FDG kinetics in small animals *Eur. J. Nucl. Med. Mol. Imag. Research* **5** 35–44
- [13] Golish S R, Hove J D, Schelbert H R, and Gambhir S S 2001 A fast nonlinear method for parametric imaging of myocardial perfusion by dynamic  $^{13}\text{N}$ -ammonia PET *J. Nuc. Med.* **42** 924–93
- [14] Golub G H, Heath M, and Wahba G 1979 Generalized cross-validation as a method for choosing a good ridge parameter *Technometrics* **21** 215–223

- [15] Gunn R N, Gunn S R, Cunningham V J 2001 Positron Emission Tomography Compartmental Models *J. Cer. Blood Flow Metab.* **21** 635–652
- [16] Huesman R H, Reutter B W, Zeng G L and Gullberg G T 1998 Kinetic parameter estimation from SPECT cone-beam projection measurements *Phys. Med. Biol.* **43** 973–982
- [17] Kamasak M E, Bouman C A, Morris E D and Sauer K 2005 Direct Reconstruction of Kinetic Parameter Images From Dynamic PET Data *IEEE Trans. Med. Imag.* **24** 636–650
- [18] Kelloff GJ, Hoffman JM, Johnson B, Scher HI et al. 2005 Progress and promise of FDG-PET imaging for cancer patient management and oncologic drug development *Clin. Cancer Res.* **11** 2785–2808
- [19] Iozzo P, Hallsten K, Oikonen V, Virtanen K, Parkkola R, Kemppainen J, Solin O, Lonnqvist F, Ferrannini E, Knuuti J and Nuutila P 2003 Effects of metformin and rosiglitazone monotherapy on insulin-mediated hepatic glucose uptake and their relation to visceral fat in type 2 diabetes *Diabetes Care* **26** 2069–2074
- [20] Lage E, Vaquero J, Sisniega A, Espana S, Tapias G, Abella M, Rodriguez-Ruano A, Ortuno J, Udas A and Desco M 2009 Design and performance evaluation of a coplanar multimodality scanner for rodent imaging *Phys. Med. Biol.* **54** 75427–5441
- [21] Limber M A, Limber M N, Cellar A, Barney J S and Borwein J M 1995 Direct reconstruction of functional parameters for dynamic SPECT *IEEE Trans. Nucl. Sci.* **42** 1249–1256
- [22] Logan J, Fowler J, Volkow N, Wolf A, Dewey S and Schlyer D 1990 Graphical analysis of reversible radioligand binding from time-activity measurements applied to n11c methylcocaine PET studies in human subjects *J. Cereb. Blood Flow Metab.* **10** 740–747
- [23] Logan J 2003 A review of graphical methods for tracer studies and strategies to reduce bias *Nucl. Med. Biol.* **30** 833–844
- [24] Massollo M, Marini C, Brignone M, Emionite L, Salani B, Riondato M et al. 2013 Metformin temporal and localized effects on gut glucose metabolism assessed using 18 F-FDG-PET in mice *J. Nuc. Med.* **54** 259–66
- [25] Meneton P, Ichikawa I, Inagami T and Schnermann J 2000 Renal physiology of the mouse *Am. J. Phys. - Renal Phys.* **278** F339–F351
- [26] Miao H, Xia X, Perelson A S and Wu H 2011 On identifiability of nonlinear ODE models and applications in viral dynamics *SIAM Rev.* **53** 3–39
- [27] Ollinger J M and Fessler J A 1997 Positron-Emission Tomography *IEEE Signal Processing Magazine* **14** 1053–5888
- [28] O’Sullivan F and Saha A 1999 Use of ridge regression for improved estimation of kinetic constants from PET data *IEEE Trans. Med. Imag.* **18** 115–125
- [29] Patlak C S and Blasberg R G 1985 Graphical evaluation of blood-to-brain transfer constants from multiple-time uptake data. Generalizations *J. Cereb. Blood Flow Metab.* **5** 584–590
- [30] Reips L, Burger M and Engbers R 2014 Towards dynamic PET reconstruction under flow conditions: parameter identification in a PDE model *arXiv:1411.5143* and submitted
- [31] Qiao H, Bai J, Chen Y and Tian J 2007 Kidney modelling for FDG excretion with PET *Int. J. Biomed. Imaging* **2007** 63234
- [32] Sanchez F, Moliner L, Correcher C, Gonzalez A, Orero A, Carles M, Soriano A, Rodriguez-Alvarez M J, Medina L A and Mora F 2012 Small animal pet scanner based on monolithic lyso crystals: performance evaluation *Med. Phy.* **39** 643–653
- [33] Schmidt K C and Turkheimer F E 2002 Kinetic modeling in positron emission tomography *Q. J. Nucl. Med. Mol. Imaging*, **46** 70–85
- [34] Shepp L and Vardi Y 1982 Maximum likelihood reconstruction for emission tomography *IEEE Trans. Med. Imag.* **1** 113–122
- [35] Shreve P D, Anzai Y and Wahl R L 1999 Pitfalls in oncologic diagnosis with FDG PET imaging: physiological and benign variants, *RadioGraphics*, **19** 61–77.
- [36] Thie J A, Smith G T and Hubner K F 1997 Linear least squares compartmental-model-independent parameter identification in PET, *IEEE Trans. Med. Imag.* **16** 11–16.

- [37] Wang G and Qi J 2013 Direct estimation of kinetic parametric images for dynamic PET *Theranostics* **3** 802–815
- [38] Tsoumpas C, Turkheimer F E and Thielemans K 2008 Study of direct and indirect parametric estimation methods of linear models in dynamic positron emission tomography *Medical Physics* **35** 1299–1309
- [39] Vanzi E, Formiconi A R, Bindi D, Cava G L and Pupi A 2004 Kinetic parameter estimation from renal measurements with a three-headed SPECT system: A simulation study *IEEE Trans. Med. Imag.* **23** 363–373
- [40] Warburg O, Wind F and Negelein E 1926 The metabolism of tumors in the body *J. Gen. Physiol.* **8** 519–530
- [41] Watabe H, Ikoma Y, Kimura Y, Naganawa M, Shidahara M 2006 PET kinetic analysis – Compartmental model *Ann. Nucl. Med.* **20** 583–588
- [42] Wernick M N and Aarsvold J N 2004 Emission Tomography: The Fundamentals of PET and SPECT *San Diego, CA: Elsevier Academic Press*
- [43] Yates J 2006 Structural identifiability of physiologically based pharmacokinetic models *J. Pharmacokinet. Pharmacodyn.* **33** 421–439
- [44] Zhou Y, Huang S C and Bergsneider M 2001 Linear ridge regression with spatial constraint for generation of parametric images in dynamic positron emission tomography studies *IEEE Trans. Nucl. Sci.* **48** 125–130
- [45] Zhou Y, Huang S C and Bergsneider M and Wong D F 2002 Improved parametric image generation using spatial-temporal analysis of dynamic PET studies *NeuroImage* **15** 697–707